Journal of Ceramic Processing Research. Vol. 14, No. 4, pp. 549~556 (2013)

J O U R N A L O F
Ceramic Processing Research

Structural and mechanical characteristics of hydroxyapatite and tri-calcium phosphates doped with Al^{3+} and F^- ions

A. Tahmasebifar and Z. Evis*
Middle East Technical University, Department of Engineering Sciences, Ankara, 06800, Turkey

In this study, doping of aluminum (Al^{3+}) and/or fluoride (F^-) ions into tri-calcium phosphate (TCP)-hydroxyapatite (HA) composites at various compositions were performed to investigate their microstructure and mechanical properties. Composites were synthesized by a precipitation method and sintered at 1100 °C for 1 hr and 5 hrs. Densities of the sintered materials were increased by extending the sintering time and increasing the amount of Al^{3+} and F^- doping. β-TCP was observed as the main phase in the composites by Rietveld refinement method. Moreover, considerable amount of HA was detected in the composites. Lattice parameters decreased upon ions substitution. Addition of doping ions resulted in smaller grains. In general, presence of Al^{3+} ions in the composites had negative effects on mechanical properties of the samples while substitution of the F^- ions improved that of the samples.

Key words: Biomaterials, Precipitation, X-ray scattering, Microstructure.

Introduction

TCP is widely used as an implant in hard tissues due to good biocompatibility and osteoconductivity whereas its poor mechanical properties limit its usage in non-load bearing areas of the body [1, 2]. β-TCP is resorbable in vivo and it is replaced with new bone growth [3]. TCP has four polymorphous, which are α, α, β and γ phases [4]. Different phases can be used in various applications depending on whether a bioresorbable or a bioactive material is desired. β-TCP is widely used as an implant due to its high resorbability in vivo when compared with other biomedical materials. K. Lin et al. studied the effect of nano-size powders and commercially produced micro-size powders on the sintering, microstructure, mechanical strength and degradability of the β-TCPs [5].

In natural calcium phosphates (CaP), there are various ions such as Mg^{2+} and Si^{4+}. TCP shows good bioactivity after doping with some trace elements; therefore, many studies were conducted about the doping of CaPs with different elements. For instance, TCP doped with silicon is used as a biodegradable material which enhances the rate of bone regeneration [6]. Sr and Mg in TCP has a great role in new bone growth. Sr promotes osteoblast function and subsequent bone formation and in low percent increases the replication of preosteoblastic cells and also enhances bone mineralization [7]. Doping of CaPs with Mg is widely studied because of its qualitative changes in bone matrix and also affected the mineral metabolism [7].

Fluorine is frequently doped to improve the thermal stability and biological properties of CaPs. It was reported that fluoride decreases the solubility/degradation in CaPs because of its high acidity resistance [8]. Seeley et al. investigated the effects of doping of TCP with NaF and CaO [8]. Density of TCP doped with 2% NaF shows 15% increase and also there are considerable increase in density of TCP doped with 2% NaF and 0.5% Ag_2O. Pure TCP has more porous structure than TCP doped with NaF [8]. Also, they exhibited that there are not a significant difference between β-TCP peaks of different compositions which means that there are not clear alterations in main phase of these ceramics due to addition of dopants [9]. However, α-TCP and HA peaks show a little change [8]. Also, it has been reported that TCP ceramics do not show cytotoxic properties on contact with extract fluids (a liquid preparation of a vegetable drug) [10]. Also, it has been observed that the amount of TCP particles and particle size strongly affect osteoblast behaviour [10]. Although, large amounts of small particles negatively affect the cell growth and cause cell death, small amount of α-TCP has a positive effect on osteoblast proliferation and expression due to the release of mineral ions such as calcium and phosphate [10]. β-TCP may cause a cell death because of the formation of intramitochondrial Ca-P crystals [10]. However, this phenomenon is rarely reported. It has been reported that doped TCPs improve osteoblast attachment and proliferation [10].

Fluoride is a trace element that affected the bone mineralization during bone formation. It was proved that the effectivity of fluoride depends on the dose of

*Corresponding author:
Tel : +90-312-210 4450
Fax: +90-312-210 4462
E-mail: evis@metu.edu.tr

fluoride and also genetic is an important factor on effectivity of fluoride in bone mineralization [11]. F^- stimulates osteoblastic activity and postpones mineralization of new bone are illustrated by Mousny et al. [11]. Mousny et al. showed that fluoride treatment did not have any influence on bone microarchitecture but it increases the osteoid formation and declines mineralization heterogeneity [11]. Also, fluoride ions affect the bone mechanical properties due to altering mineral-organic interfacial bonding [11].

It was reported that Al^{3+} ion enters to hard tissues along with Ca so it acts as an inhibitor in forming of HA in vitro [12]. For instance, it was found that increasing of the Al amount in blood plasma cause a significant decline in bone mineral density and bone mineral content of low birth infants but this is not true for full term infants indeed it is believed that in low term infants amount of Al affects the initiation and progression of bone mineralization. However, Al accelerated the formation of osteoid [12].

Although,Al^{3+} or F^- ions were separately doped into CaPs previously, no study has been found about the co-doping of TCP with Al^{3+} and F^-ions. In this study, Al^{3+} and F^- ions were co-substituted in nano CaPs for the first time. CaPs doped with Al^{3+} and F^-ions were synthesized by a precipitation method and sintered at 1100 ºC for 1 and 5 h. The heat treatment temperature selected with considering to phase diagram of $CaO\text{-}P_2O_5$ which shows that nonstoichiometric HA decomposed TCP after sintering above 900 ºC. Sintered samples were investigated by density, x-ray diffraction (XRD), scanning electron microscope (SEM), Fourier transform infrared spectroscopy (FTIR), micro-hardness and diametric tensile strength.

Experimental Procedure

Nano-TCP was synthesized by a precipitation method. Calcium nitrate tetra hydrate ($Ca(NO_3)_2{\cdot}4H_2O$) and di-ammonium hydrogen phosphate ($(NH_4)_2HPO_4$) were used as main precursors. These precursors were added into distilled water in order to prepare 0.6 M ($Ca(NO_3)_2 \cdot 4H_2O$) and 0.4 M $(NH_4)_2HPO_4$to adjust the Ca/P ratio at 1.5. Ammonia was added into the Ca-P mixture solution to adjust the pH of the final mixture to 11-12. After mixing the solution overnight, the mixture was filtered with a fine filter paper to obtain a wet cake. The wet cake was dried in the furnace at 200 ºC and sintered at 1100 ºC for 1 hr and 5 hrs.

In addition to the main precursors used in the synthesis of pure TCP, aluminum nitrate ($Al(NO_3)_3{\cdot}9H_2O$) and ammonium fluoride (NH_4F) were used to obtain aluminum and fluoride doped TCPs. 9 different compositions of pure and doped TCPs were prepared. Descriptions of pure and doped TCP samples according to their aluminum and fluoride ion compositions are summarized in Table 1.

Table 1. Description and compositions of pure and doped TCPs.

Sample ID	Mole % Al^{3+}	Mole % F^-
TCP	0	0
TCP0.5Al	0.5	0
TCP1Al	1	0
TCP2.5Al	2.5	0
TCP5Al	5	0
TCP0.5Al : 0.5F	0.5	0.5
TCP2.5Al : 1F	2.5	1
TCP2.5Al : 2.5F	2.5	2.5
TCP2.5Al : 5F	2.5	5

Density (ρ) of the materials was measured by Archimedes method using the following formula:

$$\text{Density}(g/cm^3) = \frac{Wt(air)}{Wt(air)-Wt(water)} \times \rho(water) \quad (1)$$

Where, $\rho_{(water)}$ is the density of water. Theoretical density of the pure and doped TCP was assumed to be same (3.07 g/cm^3).

XRD was used to investigate the amount of the phases and lattice parameters of the samples by using a Rigaku DMAX 2200 machine. XRD was performed on the samples with a Cu-Kα radiation at 40 kV/40 mA. The samples were scanned from 20 to 60 with 2θ angles with a scan speed of 2.0º/min. XRD results were compared with Joint Committee on Powder Diffraction Standards (JCPDS) in order to determine the positions of the diffracted planes. The amount of phases present in the samples was calculated by Rietveld analysis method. Lattice parameters of β-TCP were expressed in hexagonal form and they were calculated by successive approximation method. The unit cell volume of β-TCP was calculated by the following formula [13]:

$$V = 0.886 \cdot (a^2) \cdot c \quad (2)$$

Where, V ($Å^3$) is the volume of unit cell, a and c are the hexagonal lattice parameters in Angstroms.

Presence of bonds in the samples was investigated by FTIR. Firstly, the samples were crushed into powders by the use of a mortar and pestle. Produced ceramic powders were mixed with potassium bromide (KBr) with a weight ratio of 1/300. In order to obtain transparent pellets, the obtained powder mixture was cold pressed. The spectra records were performed from 4000 cm^{-1} to 400 cm^{-1} using a 512 scan by BioRad FTS 175 C.

The average grain size of the sintered samples was determined by SEM with a Quanta 400F equipment at a voltage of 20 kV. Intercept method was used to determine the grain size of the sintered samples [14].

The Vickers micro-hardness measurements were

performed by a Vickers micro hardness tester (HMV-2, Shimadzu, Japan). Approximately 10 measurements were performed on each sample with a diamond indenter at 200 g load for 20 seconds. The average μ-hardness was calculated by the formula below:

$$HV = 0.001854\frac{P}{d^2} \quad (3)$$

Where, HV: Vickers hardness (GPa), P: Applied load (N), d: diagonal indent length (mm).

The diametric tensile strength of sintered discs was performed by a universal testing machine (LS 500, Llyod Instruments, UK). In order to measure the diametric tensile strength, discs were located between two flat plates and compression was applied by a cylinder with a speed of 3 mm/min. During the compression, a maximum tensile strength was generated across the flat surface diameters of the discs normal to the loading direction. The tensile strength of the samples was calculated with the following formula [15]:

$$S = \frac{2F}{(\pi \cdot D \cdot t)} \quad (4)$$

Where, F: failure force, D: sample diameter, t: sample thickness.

Results and Discussion

Relative densities of pure and doped TCP sintered at 1100 ºC for 1 hr and 5 hrs are given in Table 2. All of the samples showed high densities (above 85%) after the sintering. Although densities of Al^{3+} doped samples (TCP0.5Al and TCP1Al) increased with increasing the sintering time from 1 hr to 5 hrs, densities of Al^{3+} samples (TCP2.5Al and TCP5Al) with high Al^{3+} contents decreased with extending the sintering time. However, there was no relationship between the relative density and the Al^{3+} content after the sintering for 1 hr. Sample TCP2.5Al had the highest density after the sintering for 1h. Samples doped with Al^{3+} and F^- ions were generally decreased by extending the sintering time while density of TCP2.5Al : 5F increased by extending the sintering time. Among these samples, TCP0.5Al : 0.5F sintered for 1 hr showed the highest density.

Table 2. Density of pure and doped TCPs sintered at 1100 ºC for 1hr and 5 hrs.

Sample ID	Density (g/cm^3) 1 hr	Relative Density (%) 1 hr	Density (g/cm^3) 5 hrs	Relative Density (%) 5 hrs
TCP	2.64	85.9	2.8	91.2
TCP0.5Al	2.92	95.1	2.93	95.4
TCP1Al	2.79	90.8	2.88	93.8
TCP2.5Al	2.99	99.3	2.65	86.3
TCP5Al	2.90	94.4	2.76	89.9
TCP0.5Al : 0.5F	2.98	97.0	2.82	91.8
TCP2.5Al : 1F	2.88	93.8	2.84	92.5
TCP2.5Al : 2.5F	2.91	94.7	2.89	94.1
TCP2.5Al : 5F	2.88	93.8	2.93	95.4

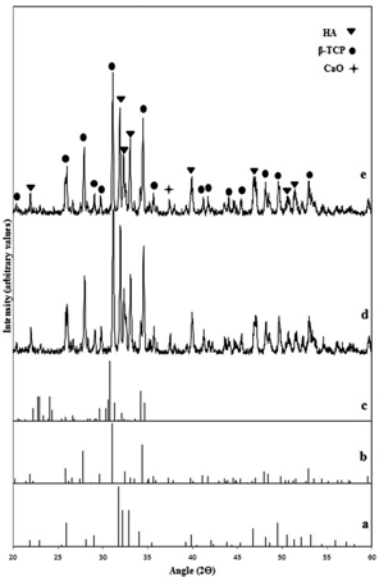

Fig 1. XRD patterns of (a) Standard HA (JCPDS#9-432), (b) Standard α-TCP (JCPDS#9-169), (c) Standard β-TCP (JCPDS#9-348), (d) TCP (sintered for 1 hr), (e) TCP (sintered for 5 hrs).

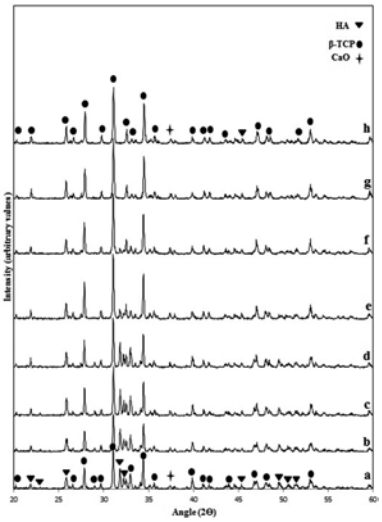

Fig. 2. XRD patterns of (a) TCP0.5Al (sintered for 1 hr), (b) TCP0.5Al (sintered for 5 hrs), (c) TCP1Al (sintered for 1 hr), (d) TCP1Al (sintered for 5 hrs), (e) TCP2.5Al (sintered for 1 hr), (f) TCP2.5Al (sintered for 5 hrs), (g) TCP5Al (sintered for 1 hr), (h) TCP5Al (sintered for 5 hrs).

XRD patterns of TCP sintered at 1100 ºC for 1 hr and 5 hrs are presented in Fig. 1. There are biphasic materials, including HA and β-TCP. Although the stoichiometric Ca/P ratio for TCP is 1.5, in our samples, we had TCP and HA biphasic materials which had a Ca/P ratio of 1.5 in the starting chemicals because of the synthesis method (precipitation method) we used, which involves high pH values during the mixing of solutions. Additionally, other parameters such as aging time and temperature affect the presence

Table 3. Presence of HA and TCP phases in the samples sintered at 1100 °C for 1 hr and 5 hrs.

Sample ID	Wt. Fraction of TCP 1hr sintered	Wt. Fraction of HA 1 hr sintered	Wt. Fraction of TCP 5 hrs sintered	Wt. Fraction of HA 5 hrs sintered
TCP0.5AL	0.538	0.462	0.547	0.453
TCP1AL	0.618	0.382	0.644	0.356
TCP2.5AL	0.859	0.141	0.874	0.126
TCP5AL	0.961	0.039	0.985	0.015
TCP0.5Al : 0.5F	0.510	0.490	0.498	0.502
TCP2.5Al : 1F	0.823	0.177	0.818	0.182
TCP2.5Al : 2.5F	0.760	0.240	0.635	0.365
TCP2.5Al : 5F	0.610	0.490	0.465	0.535

of phase in the final product [16]. Moreover, β–TCP can not be synthesized directly after the precipitation method [17]. For example, synthesized calcium deficient apatite decomposed to β-TCP after a heat treatment above 750 °C [17]. Furthermore, increasing the sintering time resulted in an increase in the amount of second phases such as TCP [18].

Rietveld analysis was applied on XRD data to detect the phase peaks more exactly and volume fraction of both phases. With the aid of GSAS program, it was found that the main phase of TCP which is sintered for 1h, is HA (61%) while the second phase is β-TCP with 39%. While, the main phase of TCP which is sintered for 5h is α-TCP with 55% and the second phase is HA. It is possible to say that HA decomposes to β-TCP after a heat treatment. This result is in correlation with the investigation of Douard et al. [17].

Doping of Al^{3+} ions into TCP resulted in β-TCP with HA phases matching with corresponding JCPDS file #s for β-TCP and HA (Fig. 2). Narrow peaks showed that increasing the Al^{3+} content increased the crystallinity of the samples. Moreover, intensity of TCP picks increased with increasing the amount of Al^{3+} ions into HA accelerates its decomposition to α and/or β-TCP. Thus, Al^{3+} ions promote the formation of TCP. According to Table 3, TCP5Al sintered for 5h has the highest weight percent of TCP. Moreover, percentage of β-TCP was increased by increasing Al^{3+} ion content so it is possible to say that Al^{3+} accelerates decomposition of HA to β-TCP.

Fig. 3 shows the XRD patterns of the samples doped with both Al^{3+} and F^- ions. All the samples are biphasic materials and the XRD patterns of these samples are matched with the standard JCPDS files for β-TCP and HA. According to Table 3, weight fraction of β-TCP is decreased by extending the sintering time in the samples doped with both Al^{3+} and F^- ions. Increase in Al^{3+} ion content causes an increase in wt. fraction of β-TCP. Hexagonal lattice parameters and unit cell volumes of the samples are shown in Table 4. Lattice parameters and unit cell parameters of the samples were decreased with increasing the sintering time as

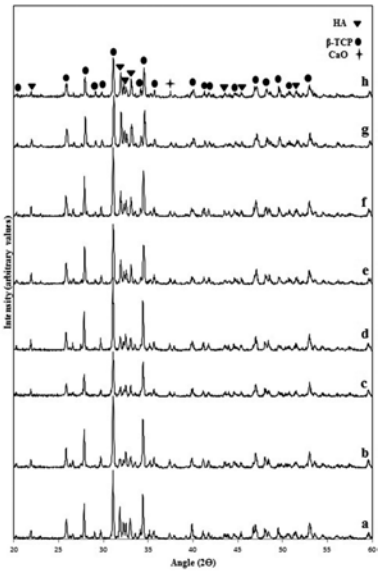

Fig. 3. XRD patterns of a) TCP0.5Al:0.5F (sintered for 1 hr), (b) TCP0.5Al : 0.5F (sintered for 5 hrs), (c) TCP2.5Al : 1F (sintered for 1 hr), (d) TCP2.5Al : 1F (sintered for 5 hrs), (e) TCP2.5Al : 2.5F (sintered for 1 hr), (f) TCP2.5Al : 2.5F (sintered for 5 hrs), (g) TCP2.5Al : 5F (sintered for 1 hr), (h) TCP2.5Al : 5F (sintered for 5 hrs).

seen in Table 4. Hexagonal lattice parameters of 'a' and 'c' decreased due to doping of TCP with Al^{3+} ions because of the difference in ionic size of Ca^{2+} (1Å) and Al^{3+}(0.53Å)ions. Therefore, substitution of Al^{3+} ions in the place of Ca^{2+} ions causes a decrease in the lattice parameters of Al doped TCPs. For each Al^{3+} ion concentration, there was a decrease in 'a' and 'c' lattice parameters as the sintering time increased.

In$Al^{3+}$and F^- co-doped samples, lattice parameters were decreased by extending the sintering time except for TCP2.5Al : 2.5F. TCP2.5Al : 5F had the smallest 'a' and 'c' both among the other samples and among the co-doped samples. TCP 2.5Al : 1F had the highest increase of 'a' lattice parameter among of all of the samples. It was proved that OH^- ions are located along the 'c' axis at the center of Ca^{2+} triangles, so substituted F^-ions lie along the 'c' axis. Also, F^- ions are more electronegative than OH^- ions [19]. Thus, increasing the F^- content may lead to an increase in

Table 4. Lattice parameters β-TCP phase of pure and doped TCPs sintered at 1100 ºC for 1 hr and 5 hrs.

Sample ID of 1 hr Sintered	a(Å)	c(Å)	V(Å^3)	ΔV(Å^3)	Sample ID of 5hrs Sintered	a(Å)	c(Å)	V(Å^3)	ΔV(Å^3)
TCP	10.4106	37.4238	3512.5	0	TCP	10.3637	37.2510	3464.8	-47.7
TCP0.5Al	10.3762	37.2092	3469.3	-43.2	TCP0.5Al	10.3462	37.1892	3459.4	-53.1
TCP1Al	10.3713	37.1744	3462.8	-49.7	TCP1Al	10.3713	37.1657	3461.9	-50.6
TCP2.5Al	10.3694	37.1900	3462.9	-49.6	TCP2.5Al	10.3685	37.1898	3462.3	-50.2
TCP5Al	10.3621	37.2486	3463.5	-49	TCP5Al	10.3598	37.0143	3440.0	-72.5
TCP0.5Al : 0.5F	10.3791	37.4681	3495.4	-17.1	TCP0.5Al : 0.5F	10.3878	37.4724	3501.6	-10.9
TCP2.5Al : 1F	10.3722	37.1913	3464.9	-47.6	TCP2.5Al : 1F	10.3715	37.1946	3464.8	-47.8
TCP2.5Al : 2.5F	10.3645	37.2510	3465.4	-47.1	TCP2.5Al : 2.5F	10.3547	37.3114	3464.4	-48.1
TCP2.5Al : 5F	10.3386	37.2698	3449.8	-62.7	TCP2.5Al : 5F	10.3299	37.2890	3445.8	-66.7

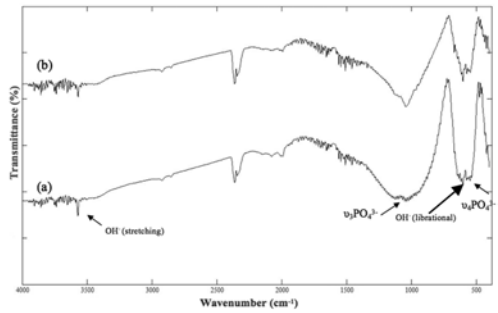

Fig. 4. FTIR patterns of (a) TCP (sintered for 1 hr), (b) TCP (sintered for 5 hrs).

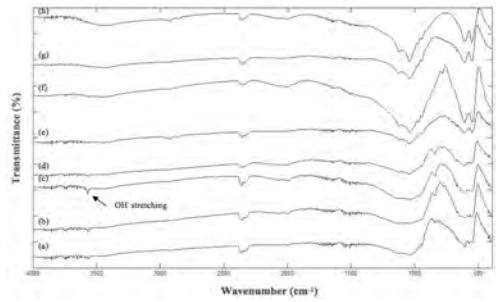

Fig. 5. FTIR pattern of (a) TCP0.5Al (sintered for 1 hr), (b) TCP0.5Al (sintered for 5 hrs), (c) TCP1Al (sintered for 1 hr), (d) TCP1Al (sintered for 5 hrs), (e) TCP2.5Al (sintered for 1 hr), (f) TCP2.5Al (sintered for 5 hrs), (g) TCP5Al (sintered for 1 hr), (h) TCP5Al (sintered for 5 hrs).

electronegativity difference between F^- ions and Ca^{2+} ions. As a result, the attraction between Ca^{2+} and F^- ions increases. Therefore, the distance between these ions decreases which leads to a decrease in 'a' axis.

The FTIR spectra of the samples are shown between Figs 4 and 6. According to Fig. 4, the bands for PO_4^{3-} group in 571 cm^{-1} which are assigned to υ_4, the triply degenerated O-P-O bending mode and in 990-1099 cm^{-1} which are assigned to υ_3, the triply degenerated asymmetric P-O stretching mode. The OH^- stretching is visible at 3572 cm^{-1} which is coming from HA. Also, the broad band of low intensity peaks is clearly visible in the range of 4000 to 3500 cm^{-1}. Thus, it is possible to say that trace amount of water incorporated into the structure of the samples [20].

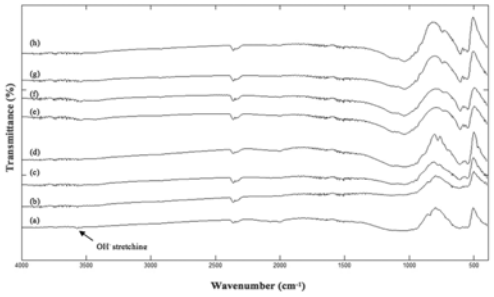

Fig. 6. FTIR pattern of (a) TCP0.5Al : 0.5F (sintered for 1 hr), (b) TCP0.5Al : 0.5F (sintered for 5 hrs), (c) TCP2.5Al : 1F (sintered for 1 hr), (d) TCP2.5Al:1F (sintered for 5 hrs), (e) TCP2.5Al : 2.5F (sintered for 1 hr), (f) TCP2.5Al : 2.5F (sintered for 5 hrs), (g) TCP2.5Al : 5F (sintered for 1 hr), (h) TCP2.5Al : 5F (sintered for 5 hrs).

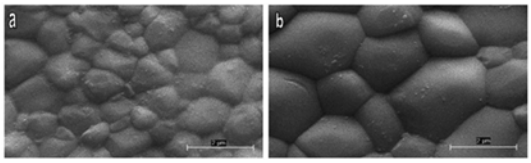

Fig. 7. SEM images of (a) TCP (sintered for 1 hr), (b) TCP (sintered for 5 hrs).

OH^- stretching and liberation band which come from HA disappeared with the increase in the Al^{3+} ion content as seen in Fig. 5. Thus, the transmittance intensities of OH^- bands decrease as the Al^{3+} ion content increase because Al accelerates the decomposition of HA to β-TCP. In addition, there are not any visible peak between 3600 and 3300 cm^{-1}. Therefore, the transformation from CaO to $Ca(OH)_2$ generally did not occur for the Al doped samples. It was reported that the presence of CaO in material which is used as an implant is so harmful due to its high reactivity against water [20]. Variation of OH^- bands give us quantitative information about HA and β-TCP. In Fig. 6, OH^- librational and PO_4^{3-} are not visible in FTIR pattern of TCP0.5Al : 0.5F. However, OH^- stretching peak is visible around 3600 cm^{-1} but its intensity is too small due to incorporation of F^- ions in the structure while the intensity of OH^- stretching was decreased by increasing F^- ions content. The peaks of PO_4^{3-} groups and OH^- librational are visible in other samples.

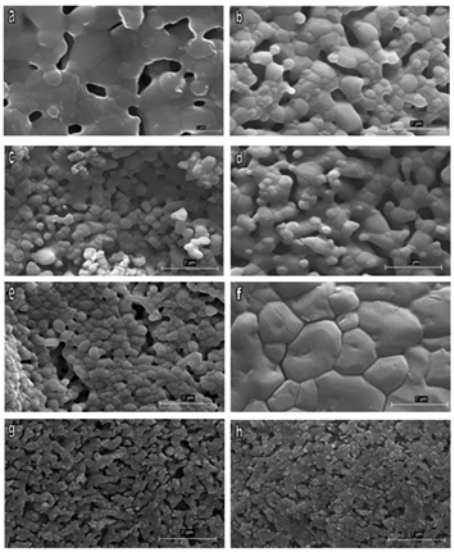

Fig. 8. SEM images of a) TCP0.5Al (sintered for 1 hr), (b) TCP0.5Al (sintered for 5 hrs), (c) TCP1Al (sintered for 1 hr), (d) TCP1Al (sintered for 5 hrs), (e) TCP2.5Al (sintered for 1 hr), (f) TCP2.5Al (sintered for 5 hrs), (g) TCP5Al (sintered for 1 hr), (h) TCP5Al (sintered for 5 hrs).

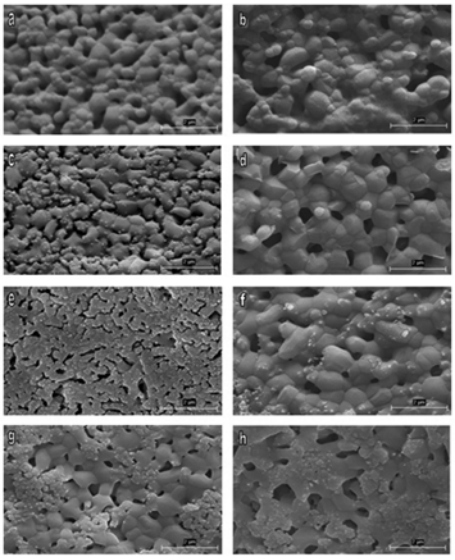

Fig. 9. SEM images of (a) TCP0.5Al : 0.5F (sintered for 1 hr), (b) TCP0.5Al : 0.5F (sintered for 5 hrs), (c) TCP2.5Al : 1F (sintered for 1 hr), (d) TCP2.5Al : 1F (sintered for 5 hrs), (e) TCP2.5Al : 2.5F (sintered for 1 hr), (f) TCP2.5Al : 2.5F (sintered for 5 hrs), (g) TCP2.5Al:5F (sintered for 1 hr), (h) TCP2.5Al : 5F (sintered for 5 hrs).

SEM images of pure and doped TCPs sintered at 1100 ºC for 1 hr and 5 hrs are presented in Figs 7 to 9. Grain size of TCP was increased by extending the sintering time (Fig. 7). There is a relationship between amount of dopant and temperature with grain sizes of apatites [21]. Grain size of HA increased the sintering time [21]. They proved that HA has a nano size grain structure after sintering at 900 and 1100 ºC [21]. According to Fig. 7, extension of sintering time has an important effect on grain size of the samples. Grain size of the samples was increased by extending the sintering time. The increase in grain size of β-TCP can be explained by attention to nucleation-aggregation-agglomeration-growth mechanism [22].

Table 5. Micro-hardness values of pure and doped TCPs at 1100 ºC for 1 hr and 5 hrs.

Sample ID	Micro-Hardness (GPa) 1 hr	Micro-Hardness (GPa) 5 hrs
TCP	4.71 ± 0.40	4.47 ± 0.28
TCP0.5Al	1.17 ± 0.09	1.40 ± 0.11
TCP1Al	2.80 ± 0.03	2.31 ± 0.02
TCP2.5Al	1.84 ± 0.04	1.47 ± 0.03
TCP5Al	1.30 ± 0.02	1.09 ± 0.00
TCP0.5Al : 0.5F	1.41 ± 0.09	1.34 ± 0.10
TCP2.5Al : 1F	0.37 ± 0.03	0.37 ± 0.03
TCP2.5Al : 2.5F	0.49 ± 0.05	0.40 ± 0.04
TCP2.5Al : 5F	0.44 ± 0.01	0.42 ± 0.01

Table 6. Diametral tensile strength values of pure and doped TCPs at 1100 ºC for 1 hr and 5 hrs.

Sample ID	Tensile Strength (MPa) 1 hr	Tensile Strength (MPa) 5 hrs
TCP	3.82 ± 1.73	2.85 ± 1.03
TCP0.5Al	4.01 ± 1.80	3.74 ± 1.68
TCP1Al	6.09 ± 2.03	5.53 ± 1.42
TCP2.5Al	7.01 ± 2.24	5.85 ± 2.50
TCP5Al	8.11 ± 2.19	6.83 ± 2.15
TCP0.5Al : 0.5F	8.50 ± 2.69	7.62 ± 1.68
TCP2.5Al : 1F	7.04 ± 2.81	4.27 ± 1.60
TCP2.5Al : 2.5F	9.81 ± 2.83	6.38 ± 2.80
TCP2.5Al : 5F	8.01 ± 1.92	5.42 ± 2.01

According to Figure 8, doping of TCP with Al^{3+} had significant effect on grain size of the samples. Samples doped with Al^{3+} ions had porous structure and this porosity had a direct relation with the increase in the content of Al^{3+} ions. SEM images showed that porosity of the samples increased by increasing the Al^{3+} ions content. According to these images, grain size of the samples was decreased in comparison to pure TCP and this decrease in grain size was increased by increasing Al^{3+} content. The degree of decomposition has a significant effect on morphological structure of the samples [23]. As a consequence, an increase in the degree of decomposition negatively affected the densification of the samples.Al^{3+} doped TCPs is porous because of the reaction between HA and TCP. Since Al^{3+} accelerates decomposition of HA to TCP, increasing Al^{3+}ion content cause an increase in porosity of the samples. It was reported that the doping of HA with Y^{3+} and F^- prevented decomposition of HA to TCP and resulted in an increase in density [21]. Al^{3+} and F^-doped samples had porous structure and also smaller grain size when compared with pure TCP as seen in Fig. 9. There are lots of pores throughout the surfaces of the samples indicating the poor densification of the samples doped with Al^{3+} and F^- ions. According to Fig. 9(a) and (c) the porosity of the sample was increased by

increasing the Al^{3+} concentration.

Micro-hardness of the samples was decreased by extending the sintering time are seen in Table 5. While TCP0.5Al showed an increase in micro hardness after extending the sintering time, Increasing the sintering time negatively affected the mechanical properties of the other samples. It was reported that the hardness of HA and FHA was increased by increasing the sintering temperature but a decrease was observed with increasing the degree of fluoridation [24]. Indeed the hardness of samples with higher degree of fluoridation exhibits a decrease by increasing the sintering temperature [24]. As seen in Table 5, samples doped with Al^{3+} ions show a great decrease in micro-hardness due to their highly porous structure. In co-doped samples, TCP0.5Al : 0.5F has the highest micro-hardness while TCP2.5Al : 1F shows the smallest micro-hardness.

Table 6 exhibits the diametric tensile strength test results. According to this table, there is a decrease in tensile strength values by extending the sintering time. Increasing the grain size had negative effect on mechanical properties of the samples. Previous studies showed that tensile strength values depend on different factors such as porosity, contact area, diameter, thickness, poisson ratio, grain size and distribution of the pores in the samples [15, 25]. It was reported that increasing the relative density has a positive effect of diametric tensile strength of HA, indeed there is an increase in tensile strength of HA by increasing the relative density of the samples [26]. Also, presence of second phase has a considerable effect on tensile strength values. Theoretical tensile strength that was reported for completely dense HA is around 35 MPa while for HA which has open pore structure; this value is around 1-2 MPa [27].

Presence of second phase might decrease the mechanical properties of ceramics. For example, presence of β-TCP and HA as a second phase declined the mechanical properties of biphasic biomaterials [28]. However, biphasic ceramics are widely used as biomaterials due to their good biological reactivity and bonding with bone in comparison with pure ceramics [20, 29]. Also, β-TCP improves the mechanical properties of the samples because of its high rate of dissolution, which promotes bone in-growth [20, 29]. In Al doped samples, there is a correlation among the tensile strength values and relative densities of the samples except for TCP5Al and TCP1Al. TCP2.5Al had the highest relative density and the smallest grain size while TCP5Al had the highest tensile strength value. This phenomenon might be explained by considering the influence of second phase on mechanical properties of the samples. In co-doped samples, TCP2.5Al : 2.5F had the highest tensile strength value and the smallest grain size.

Conclusion

In this study, TCP was synthesized by a precipitation method and doped with Al^{3+} and/or F^- ions in order to investigate its microstructural and mechanical properties. Density of the samples doped with Al^{3+}ions shows a considerable increase. However, the densification of the samples decreased by extending the sintering time except for TCP1Al and TCP0.5Al. Structural analysis determined by Rietveld refinement proved the presence of β-TCP as the main phase and HA resulting in the formation of HA/β-TCP biphasic composites. Lattice parameters decreased upon ions substitution. SEM results showed that addition of doping ions resulted in smaller grains. In addition to characteristic bands of TCP, F^- ion substitution was confirmed. In general, Al^{3+} ions in large amounts had negative effects on the mechanical properties of the samples, while substitution of the F^- ions improved the mechanical properties of the samples.

References

1. S. Ni and J. Chang, J. Biomater. Appl. 24 (2009). 139-158.
2. M. Descamps, O. Richart, P. Hardouin, J.C. Hornez and A. Leriche, Ceram. Inter. 34 (2008). 131-1137.
3. K.P. Sanosh, M.-C. Chu, A. Balakrishnan, T.N. Kim and S.-J. Cho, Current Appl. Phys. 10 (2010) 68-71.
4. K. Sugiyama and M. Tokonami, *Phys.* Chem. Minerals. 15 (1987). 125-130.
5. K. Lin, J. Chang, J. Lu, W. Wu and Y. Zeng, Ceram. Inter. 33 (2007) 979-985.
6. I.M. Martinez, P.A. Valasquez and P.N. De Aza, Mater. Charact. 61 (2010) 761-767.
7. S.S. Banerjee, S. Tarafder, N.M. Davies, A. Bandyopadhyay and S. Bose, Acta Biomaterialia. 6 (2010) 4167-4174.
8. Z. Seeley, A. Bandyopadhyay and S. Bose,Mater. Sci. Eng. C 28 (2008)11-17.
9. A. Bignon, J. Chouteau, J. Chevalier, G. Fantozzi, J.-P. Carret, P. Chavassieux, G. Boivin, M Melin and D. Hartmann, J. Mater. Sci.: Mater. Med. 14 (2003). 1089-1097.
10. T. Kokubo, Bioceramics and their clinical applications (CRC Press, 2008). p. 92.
11. M. Mousny, S. Omelon, L. Wise, E.T. Everett, M. Dumitriu, D.P. Holmyrad, X. Banse, J.P. Devogealer and M.D. Grynpas, Bone. 43 (2008). 1067-1074.
12. W.G. Goodman and M.E. Duarte, Mineral and Electrolyte Metabolism. 17 (1991). 221-232.
13. B.D. Cullity, Elements of X-ray Diffraction, Second Ed. (Addison-Wesley Publishing Company,1978). p. 501.
14. J.E. Hilliard, Metal Progress Data Sheet. (1964). 99-102.
15. Z. Evis and F. Ozturk, Mater. Sci. Tech. 24 (2008). 474-478.
16. M. Descamps, J.C. Hornez and A. Leriche, J. Eur. Ceram. Soc. 27 (2007). 2401-2406.
17. N. Douard, R. Detsch, R. Chotard-Ghodsnia, C. Damia, U. Deisinger and E. Champion, Mater. Sci. Eng. C. 31 (2011). 531-539.
18. P.E. Wang and T.K. Chaki, Bioceramics: Materials and Applications, edited by G. Fischman, A. Clare and L.

Hench (Ceramic Transactions, 48,1995). p. 225.
19. K.A. Gross and L.M. Rodriguez-Lorenzo, Biomater. 25 (2004) 1375-1384.
20. A. Slosarczyk, C. Paluszkiewicz, M. Gawlicki and Z. Paszkiewicz, Ceram. Inter. 23 (1997) 297-304.
21. B. Basar, A. Tezcaner, D. Keskin and Z. Evis, Ceram. Inter. 36 (2010) 1633-1643.
22. Z. Evis, J. Ceram. Soc. Japan. 114 (2006) 1001-1004.
23. H.-W. Kim, Y.-J. Noh, Y.-H. Koh and H.-E. Kim, J. Mater. Sci.: Mater. Med. 14 (2003) 899-904.
24. H. Eslami, M. Solati-Hashjin and M. Tahriri, Mater. Sci. Eng. C. 29 (2009) 1387-1398.
25. K.T. Chau and X.X. Wei, Inter. J. Solids Structures. 38 (2001) 1459-1481.
26. A. Bigi, E. Foresti, R. Gregorini, A. Ripamonti, N. Roveri and J.S. Shah, Calcified Tissue Inter. 50 (1992) 439-444.
27. V.S. Komlev, S.M. Barinov and F. Rustichelli, J. Mater. Sci. Lett. 22 (2003) 1215-1217.
28. S. Best, W. Bonfield and C. Doyle, Proceedings of the Second International Symposium on Ceramics in Medicine, edited by G. Heimke (Heidelberg, Germany,1989). p. 57.
29. S. Kannan and J.M.F. Ferreira, Chem. Mater. 18 (2006) 198-203.